Published in final edited form as:
Toxicol Appl Pharmacol. 2010 November 1; 248(3): 249–258. doi:10.1016/j.taap.2010.08.008.

Fullerenol Cytotoxicity in Kidney Cells is Associated with Cytoskeleton Disruption, Autophagic Vacuole Accumulation, and Mitochondrial Dysfunction

Denise N. Johnson-Lyles[a], **Kimberly Peifley**[b], **Stephen Lockett**[b], **Barry W. Neun**[a], **Matthew Hansen**[a], **Jeffrey Clogston**[a], **Stephan T. Stern**[a,*], and **Scott E. McNeil**[a]

[a]Nanotechnology Characterization Lab (NCL), Advanced Technology Program, SAIC-Frederick, Inc., NCI-Frederick, Frederick, Maryland 21702

[b]Optical Microscopy Analysis Lab (OMAL), Advanced Technology Program, SAIC-Frederick, Inc., NCI-Frederick, Frederick, Maryland 21702

Abstract

Water soluble fullerenes, such as the hydroxylated fullerene, fullerenol ($C_{60}OH_x$), are currently under development for diagnostic and therapeutic biomedical applications in the field of nanotechnology. These molecules have been shown to undergo urinary clearance, yet there is limited data available on their renal biocompatibility. Here we examine the biological responses of renal proximal tubule cells (LLC-PK1) exposed to fullerenol. Fullerenol was found to be cytotoxic in the millimolar range, with viability assessed by the sulforhodamine B and trypan blue assays. Fullerenol-induced cell death was associated with cytoskeleton disruption and autophagic vacuole accumulation. Interaction with the autophagy pathway was evaluated *in vitro* by Lysotracker Red dye uptake, LC3-II marker expression and TEM. Fullerenol treatment also resulted in coincident loss of cellular mitochondrial membrane potential and ATP depletion, as measured by the Mitotracker Red dye and the luciferin-luciferase assays, respectively. Fullerenol-induced ATP depletion and loss of mitochondrial potential were partially ameliorated by co-treatment with the autophagy inhibitor, 3-methyladenine. *In vitro* fullerenol treatment did not result in appreciable oxidative stress, as measured by lipid peroxide and glutathione content. Based on these data, it is hypothesized that cytoskeleton disruption may be an initiating event in fullerenol cytotoxicity, leading to subsequent autophagy dysfunction and loss of mitochondrial capacity. As nanoparticle-induced cytoskeleton disruption, autophagic vacuole accumulation and mitochondrial dysfunction are commonly reported in the literature, the proposed mechanism may be relevant for a variety of nanomaterials.

Keywords

fullerenol; autophagy; mitochondrial dysfunction

*Corresponding author, contact info: Stephan T. Stern, National Cancer Institute at Frederick, Post Office Box B, Frederick, MD 21702, Phone: 301-846-6198, Fax: 301-846-6399, sternstephan@mail.nih.gov.

Introduction

Fullerenols, hydroxylated derivatives of carbon fullerenes, have been documented in the literature to possess significant *in vitro* and *in vivo* antioxidant and free-radical scavenging capabilities (Bensasson, *et al.*, 2000; Dugan, *et al.*, 1997; Gharbi, *et al.*, 2005; Okuda, *et al.*, 1996; Wang, *et al.*, 1999; Xiao, *et al.*, 2005). Numerous studies have been conducted to evaluate the therapeutic potential of fullerenol compounds against oxidative stress-associated conditions, including cancers, cardiotoxicity, hepatoxicity, and nephrotoxicity (Injac *et al.*, 2008a; Injac *et al.*, 2008b; Injac *et al.*, 2008c; Injac *et al.*, 2009; Harhaji *et al.*, 2007). MRI contrast agents based on gadolinium containing endohedral metallofullerenols are of particular interest in the clinical setting due to their high water proton relaxivity properties (Anderson *et al.*, 2006; Bolskar *et al.*, 2008; Zang *et al.*, 2007b). Adding to their clinical utility, these molecules and other carbon based nanoplatforms are also being evaluated for intravascular delivery of drugs and diagnostics (Chaudhuri *et al.*, 2009; Peer *et al.*, 2007). Despite the potential, wide-spread biomedical applications of fullerenol, there is limited data available on its biocompatibility. Although most of the scientific literature supports a protective role of fullerenol in biological systems, there is a growing body of literature detailing the cytotoxic effects of this nanoparticle (Yamawaki and Iwai, 2006; Ueng *et al.*, 1997; Su *et al.*, 2009; Sayes, *et al.*, 2004). Fullerenol has been reported to decrease endothelial cell density, to decrease cell proliferation and cell attachment, to promote LDH release, and to increase accumulation of polyubiquitinated proteins (Yamawaki and Iwai, 2006). Water soluble fullerene derivatives have been reported to cause cell cycle arrest at the G1 phase in Chinese hamster lung and ovary cells (Su *et al.*, 2009). Derivatized fullerenes have also been reported to exhibit differential cytotoxicity in human dermal fibroblasts and liver carcinoma cell lines, with the more water soluble derivatives demonstrating lesser adverse effects in culture (Sayes, *et al.*, 2004).

The kidney is a major organ responsible for the elimination of drugs and their metabolites (Verbeeck and Musuamba, 2009; Perazella, 2009). The derivatization of fullerene to fullerenol has been shown in rodent models to shift biodistribution and excretion profiles from one of primarily liver localization and fecal excretion to multi-organ localization (primarily liver, kidney, spleen, bone) and urinary excretion (Yamago *et al.*, 1995; Qingnuan *et al.*, 2002). Currently there are no reports in the literature of the evaluation of fullerene cytotoxicity in kidney cells (*in vitro or ex vivo*), and few reports on plausible cellular targets of this nanomaterial within cells. Given the *in vivo* exposure of kidneys to fullerenol following parenteral administration, assessing *in vitro* and *in vivo* renal responses to fullerenol are important steps in evaluating the safety of this material.

In this present study, *in vitro* renal cell responses to fullerenol exposure were evaluated in the porcine proximal tubule cell model, LLC-PK1, as an initial step in examining fullerenol renal cell toxicity. The LLC-PK1 cell line has both structure and function similar to cells of the proximal tubule and have been used to study adverse effects of a number of nephrotoxicants (Pfaller and Gstraunthaler, 1998; Williams 1989). The results reported herein, detail extensive characterization on the biochemical and morphological effects of fullerenol on kidney cells and highlight the importance of thorough biological characterization of nanotechnology based drug and diagnostic platforms prior to their clinical use. As the findings of cytoskeleton disruption, autophagic vacuole accumulation, and mitochondrial potential loss have been reported for a variety of nanomaterials, fullerenol may also serve as a model nanoparticle for evaluating the underlying mechanism of nanomaterial cellular toxicity.

Materials and Methods

Materials

Fullerenol (Part# M16) was purchased from Materials and Electrochemical Research Corporation (Tucson, AZ). Bovine serum albumin, 1-butanol, butylated hydroxytoluene, 3-methyl adenine, Costar six well and ninety-six well, flat-bottomed, cell culture plates, dimethyl sulfoxide, diethyl maleate, 5-5'-dithiobis(2-nitrobenzoic acid), glycine, malondialdehyde tetraethylacetal (1,1,3,3 tetraethoxypropane), methanol, β-nicotinamide adenine dinucleotide 2'-phosphate reduced tetrasodium salt, ethylenediaminetetraacetic acid tetrasodium salt dehydrate, oxidized glutathione, protease inhibitor cocktail, phenyl methyl sulphonyl fluoride, 5-sulfosalicyclic acid dehydrate, sodium phosphate, sodium carbonate, sodium chloride, sulforhodamine B dye, Hank's balanced salt solution with calcium and magnesium, Hoechst dye, thiobarbituric acid, trichloroacetic acid, Trypan Blue, Triton-X-100, and Tween-20 were purchased from Sigma-Aldrich, Inc. (St. Louis, MO). *L*-glutamine, RPMI-1640 (phenol free), and bovine serum were purchased from Hyclone, Inc. (Logan, UT). Medium 199 (M199) media was purchased from Cambrex (East Rutherford, NJ). Quick start Bradford dye reagent 1X was purchased from Bio-Rad Laboratories, Inc. (Hercules, CA). Carbon rods, dodecenylsuccinic acid, embed-812, sodium acetate, sodium cacodylate, osmium tetroxide, and uranyl acetate were purchased from Electron Microscopy Sciences (Hatfield, PA). Ethanol (190 and 200 proof) was purchased from Pharmco (Brookfield, CT). Lead citrate was purchased from Laurylab (Saint-Fons Cedex, France). Cell extraction buffer, Hank's balanced salt solution (with calcium and magnesium), NuPAGE LDS 4X sample buffer with reducing agent (10X), SeeBlue® Plus2 prestained standard, 4–20% tris-glycine gels, tris-glycine running buffer (10X), transfer buffer (25X), Lysotracker Red DND-99, Mitotracker Red CMX-Ros, Oregon Green 488 phalloidin, and Celltracker Green CMFDA were purchased from Invitrogen, Inc. (Carlsbad, CA). Westran S polyvinylidene fluoride (PVDF) protein blotting membrane, blotting paper, and 18 mm coverglass (coverslips) were purchased from Fisher Scientific, Inc. (Pittsburgh, PA). Tris-buffered saline (25X) was purchased from Amresco, Inc. (Solon, OH). Bicinchoninic acid (BCA) protein assay, StartingBlock blocking buffer, and electrochemiluminescent (ECL) western blotting substrate reagent were purchased from Pierce (Rockford, IL). Mouse monoclonal anti-LC3 antibody was purchased from NanoTools (Teningen, Baden-Württemberg, DE). Peroxidase-conjugated AffiniPure donkey anti-mouse IgG was purchased from Jackson ImmunoResearch Labs, Inc. (Westgrove, PA). Hyperfilm ECL was purchased from Amersham Biosciences, Inc. (Piscataway, NJ). CellTiter-Glo Luminescent Cell Viability Assay Kit was purchased from Promega, Corp. (Madison, WI). All other chemicals and reagents were obtained from Fisher Chemical Co. (Fair Lawn, NJ) or one of the above suppliers, and all were of reagent grade or better.

Fullerenol Physicochemical Characterization

Elemental analysis (carbon, hydrogen, oxygen, and sodium), inductively coupled plasma-mass spectrometry (ICP-MS), and Fourier transform infrared spectroscopy (FT-IR) analyses were conducted on batch-matched fullerenol samples for empirical molecular formula determination (elemental analysis), inorganic and organic sample impurity assessment (ICP-MS and FT-IR), and structure characterization (FT-IR). Detailed methods and results for elemental and ICP-MS analyses can be found in the Supplemental Data section of this manuscript. FT-IR analyses demonstrated a C-O vibration at 1054 cm^{-1}, a strong O-H vibration at 1360 cm^{-1}, a very strong O-H stretch at 3217 cm^{-1}, and a C=C vibration band at 1575 cm^{-1}. These IR values are consistent with previous reports by Xing, *et al.*, 2004 for fullerenol structural properties.

Hydrodynamic Size by Dynamic Light Scattering (DLS)

Fullerenol was weighed and dissolved in 10 mM NaCl or PBS to give a final concentration of 25 mM. Samples were passed through a 0.02 μm filter. Hydrodynamic size (diameter)

measurements were performed in batch mode at 25°C in a low volume quartz cuvette using the Malvern Zetasizer Nano ZS instrument with a back scattering detector. A minimum of twelve measurements were made per sample. Intensity-weighted average was used to determine hydrodynamic size, while volume distribution data was used to determine relative amounts.

Cell Line Maintenance

The porcine renal proximal cell line (LLC-PK1 cells, American Type Culture Collection, Rockville, MD) was maintained in 95% air/5% CO_2 environment at 37°C in M199 media with 3% fetal bovine serum (complete media). The cells were split 1:5, and passage number was limited to 20 passages.

Sulforhodamine B (SRB) Cell Viability Assay

Cells were plated at a density of 25,000/well in 96-well format. Cells were grown for 24 hrs, reaching a confluence of 80%, prior to treatment in triplicate with fullerenol (0.0002–60 mM) or media control for 24 and 48 hrs. After treatment, dose media was aspirated, 200 μL of fresh media and 50 μL of trichloroacetic acid (TCA) solution (50% w/v in H_2O) were added to all wells. The plates were incubated at 4°C for 10 min for TCA cell fixation. Following fixation, the TCA solution was removed and cell plates were washed with deionized water and allowed to dry at ambient temperature. After the plates were completely dry, cells were stained with SRB (0.4% in acetic acid, 100 μL/well) for 10 min and the plates were washed with deionized water to remove excess unbound dye. SRB was extracted from dry, stained cells by the addition of 200 μL of Tris base (10 mM). Absorbance was read at 510 nm on a microplate spectrophotometer. Viability was expressed as percent media treated control.

ATP Assay

Cellular ATP content was measured using the CellTiter-Glo Luminescent Cell Viability Kit (Promega Cat. #G7571). This assay quantifies cellular ATP content in a homogeneous format by measuring the luminescent signal catalyzed by the addition of luciferin substrate, proprietary recombinant luciferase, and kit reaction buffer to lyse cells. The luminescent signal is the direct result of mono-oxygenation of the luciferin substrate and is dependent upon the presence of magnesium, ATP (from lysed cells), and oxygen. LLC-PK1 cells were plated in a 96-well format (25,000 cells/well), grown to 80% confluence, and were either pre-treated in triplicate with 2 mM 3-methyladenine (3-MA) for 2 hours prior to addition of 0.2–60 mM fullerenol for an additional 24 and 48 hrs, or were directly treated in triplicate with 0.2–60 mM fullerenol or media control for 24 and 48 hrs. Final 3-MA concentration following fullerenol addition for all experiments was 1 mM. Dosing media was aspirated at each time point, cells were washed once with M199 media, and manufacturer kit instructions were followed to determine ATP content by luminescence measurement.

Protein Determination

Bradford Assay—Cellular protein was determined using the Quick Start Bradford Dye Reagent, 1X kit from Bio-Rad Laboratories, Inc. Cellular protein pellets from the reduced glutathione and lipid peroxidation assays were resuspended in 0.5 mL of 0.05 N NaOH. For protein quantitation, a BSA standard curve from 0.125 to 1.0 mg/mL was prepared in 0.05 N NaOH. A 5 μL sample of the BSA standard, cellular protein sample, or 0.05 N NaOH blank was added to wells of a 96-well microtiter plate in duplicate. Next, 250 μL of 1X Bradford dye reagent was added to each well, the plate was gently vortexed using an orbital shaker, then incubated at room temperature for 30 min. Following incubation, the plate was read at 595 nm on a microplate spectrophotometer.

BCA Assay—Cell lysate protein concentrations for LC3 western blot analysis were determined using the Pierce BCA protein assay. The working reagent was prepared according to product instructions by mixing 25 parts of Micro BCA™ Reagent MA and 24 parts Reagent MB with one part of Reagent MC (25:24:1, Reagent MA:MB:MC). The standard curves for the cell lysates were prepared in their respective cell extraction buffers using BSA, from 0.5 to 200.0 μg/mL. A 150 μL sample of each standard, unknown, or extraction buffer blank was transferred to the microplate wells in duplicate. To these sample wells, 150 μL of the working reagent was added, and the plate was gently mixed on an orbital shaker for 30 s. The plate was then covered and incubated at 37°C for 2 hrs. Following incubation, the plate was allowed to cool to room temperature, and the absorbance was measured at 562 nm on a microplate spectrophotometer.

TEM Microscopy—LLC-PK1 cells were seeded in 6-well chambers at a density of 62,500 cells/mL. Cells were pre-incubated for 24 hrs prior to addition of test sample, reaching an approximate confluence of 40%. Cells were then treated in triplicate for 6 hrs with media (negative control), Hanks balanced salt starvation media (positive control), or 0.03 mM fullerenol. Cells were washed with media two times prior to fixing them in TEM fixative solution (4 % formaldehyde, 2 % glutaraldehyde in 0.1 M sodium cacodylate buffer). Fixed cells were kept a room temperature for 1 hr, then transferred to 4°C prior to being post-fixed in osmium tetroxide (1% OsO_4 in 0.1 M cacodylate buffer) and uranyl acetate (0.5% uranyl acetate in 0.1 N acetate buffer), dehydrated step-wise in ethanol, and embedded in embed-182 epoxy resin for TEM imaging. Upon solidification of the resin, resin blocks were removed with a jeweler's saw and affixed to a blank resin block. The face of the block was trimmed down to approximately 1 mm square and placed into an ultramicrotome. Thin sections (70 to 90 nm thin sections) were trimmed with a diamond knife, and transferred onto copper-mesh grids cleaned by ultrasonication. Sections were stained with 3% uranyl acetate and lead citrate. Stained samples were then carbon coated, and placed into a Hitachi H7600 microscope running at 80 kV voltage to acquire TEM images. The magnification range was (200x–200,000x).

Mitochondria and Actin Confocal Microscopy—LLC-PK1 cells were plated on 18 mm sterile coverslips at a density of 1.0×10^5 cells/mL in 35 mm culture dishes (1 mL of cells per coverslip) and were grown to approximately 80% confluence overnight. After incubation overnight, cell culture coverslip samples were treated with fullerenol (0.6 or 3 mM in complete media), with nocodazole (50 μM in complete media) or complete media. Nocodazole was included as a positive control for actin disruption. Following treatment, cells were washed with phenol-free complete media, stained with Mitotracker Red CMX-Ros (200 nM in phenol-free complete media) for 30 min at 37°C, and washed again with phenol-free complete media prior to fixation with 4 % formaldehyde (in phenol-free complete media). For actin staining, cells were fixed in 4% formaldehyde solution in PBS for 10 minutes at room temperature, washed two times with PBS, and extracted with 0.1% Triton X-100 (in PBS) for 3–5 min at ambient temperature. Next, cells were pre-incubated with 1% BSA (in PBS) for 20 min at ambient temperature, and then stained with 1 unit (fluorescence) of Oregon Green 488 phalloidin dye/ Hoechst nuclear stain/coverslip (20 μL of 6.6 uM methanolic Oregon Green stock solution/5 μg Hoechst/mL of 1% BSA-PBS /coverslip) for 20 min at ambient temperature. A methanolic stock of Oregon Green 488 phalloidin dye (approximately 200 units/mL or 6.6 μM) was prepared according to manufacturer's instructions prior to preparation of the dye working solution in 1% BSA-PBS for cell culture experiments. Prior to confocal imaging, inverted coverslips were mounted onto standard glass microscope slides. Confocal images were acquired with a Zeiss LSM 510 confocal microscope. The band pass filter sets used were excitation at 405 nm with band pass emission filters 390–465 nm for Hoechst, excitation at 488 nm with band pass emission filters 500–550 nm for Oregon Green, and excitation at 543

nm with a long pass filter of 560 nm for Mitotracker Red. A uniform Mitotracker Red detector gain setting of 604 was used for all images.

Lysotracker Red Dye Uptake Assay—The Lysotracker Red assay is based on the method of Rodriguez-Enriquez et al. (2006). Modifications include substitution of a 96-well plating format for the 48-well, altered Lysotracker Red dye incubation conditions, elimination of the cell fixation step, and addition of Celltracker Green CMFDA dye for normalization to viable cell number. Lysotracker Red DND-99 is a cationic fluorescent dye that preferentially accumulates in the acidic lysosomal compartments. The amount of dye taken up by cells in culture can be used as an indicator of lysosome content and an indirect measure of autophagolysosome. Celltracker Green is deacetylated within viable cells to a thiol-reactive dye that remains in cytosol and is used to normalize the Lysotracker signal to viable cells. LLC-PK1 cells were plated at a density of 1.0×10^5 cells/mL in 96-well format and grown to approximately 80% confluence. Following cell attachment, cells were treated in triplicate with 0.01–6 mM fullerenol, with or without 3-MA. For 3-MA and fullerenol co-treatment, cells were pretreated with 2 mM 3-MA (in M199 media with 3% fetal bovine serum) before addition of fullerenol. Final 3-MA concentration following fullerenol addition for all experiments was 1 mM. After each treatment period, plated cells were processed according to Stern *et al.*, (2008). Briefly, treated cells were washed and then stained with 100 μL of 50 nM Lysotracker Red/10 μM Celltracker Green co-staining solution prepared in phenol-free RPMI-1640 for 1 hr at 37°C. Following dye uptake, the co-staining was removed and plates were rinsed twice with 200 μL of phenol-free RPMI, and 200 μL of phenol-free RPMI was added to each plate well. Lysotracker Red fluorescence (λ_{max} = 590 nm) and Celltracker Green fluorescence (λ_{max} = 517 nm) were measured using a microtiter plate reader. Lysotracker Red uptake for treated cells were expressed as the ratio percent of control, normalized to Celltracker Green (percent control Lysotracker Red fluorescence/percent control Celltracker Green fluorescence).

LC3 Immunoblot—This assay measures lipidation of microtubule associated protein LC3-I to LC3-II by immunoblot. The amount of LC3-II expression is used as a marker of autophagy (Klionsky, *et al.*, 2007). LLC-PK1 cells were treated in T-75 flasks with positive control (Hank's balanced salt solution with 1.3 mM calcium and 0.9 mM magnesium, negative control (complete media), or 6 mM fullerenol in duplicate for 6 and 24 hrs. Cell lysates were processed according to Stern *et al*. (2008) and the protein content in the cell lysate samples was determined by the BCA protein assay. Equal protein quantities of cell lysates were diluted in 4X NuPAGE buffer, vortexed, heated at 95°C for 5 min, and centrifuged at maximum speed (18,000 x g) for 30 min before loading onto 4–20% tris-glycine gels. The gels were run at 125 V for approximately 2 hrs, rinsed with deionized water, and transferred to PVDF membranes overnight at 30 mA. The transfer membrane was washed 3 times with 50–100 mL of tris-buffered saline (TBS) (0.01% Tween 20) for approximately 15 min each, and blocked with 50 mL StartingBlock blocking buffer (0.01% Tween-20) at room temperature for approximately 1 hr. The membrane was then incubated with anti-LC3 primary antibody solution (1:200 dilution in 5 mL of the StartingBlock blocking buffer) for 2 hr at room temperature, using hybridization bags cut to size. The membrane was then washed twice with 50–100 mL of TBS (0.01% Tween 20), for 15 min each, and incubated with the secondary donkey anti-mouse IgG-HRP conjugate (1:50,000 dilution in StartingBlock blocking buffer) for 1 hr at room temperature. The membrane was washed twice with 50–100 mL of TBS (0.01% Tween 20), for 15 min each, incubated with 3 mL ECL peroxidase substrate solution (1:1 peroxidase substrate to luminol enhancer solution) for approximately 1 min, and the immunoblot was developed for 8 min using Hyperfilm ECL.

Statistics—Statistical analyses were conducted using the software program Statistica version 7.1 (StatSoft, Inc., Tulsa, OK). Statistical differences ($p \leq 0.05$) were determined by Student's t-test, or ANOVA and Dunnett's post hoc.

Results

Hydrodynamic Size and Zeta Potential of Fullerenol

The mean intensity and volume size distributions of filtered fullerenol samples in PBS and 10 mM NaCl were determined by Dynamic Light Scattering (DLS) (Figure 1). The theoretical hydrodynamic size of fullerenol is approximately 2 nm. In this study, fullerenol-PBS samples exhibited a bi-modal size distribution by intensity, with a small peak at 20 nm accounting for approximately 97.8% of the total particle volume. Given the theoretical size of fullerenol, this 20 nm peak is indicative of fullerenol aggregates that were formed during DLS sample preparation. Although fullerenol is highly soluble in aqueous solutions, these particles can aggregate and gradually precipitate out of solution during the course of DLS sample preparation and measurement. The larger fullerenol-PBS intensity peak at 500 nm was primarily due to larger aggregates and only corresponded to approximately 2.2% of the total particle volume. In contrast to fullerenol-PBS samples, fullerenol particles prepared in 10mM NaCl did not appear to aggregate as greatly in solution. This difference in aggregation tendency may be attributed to the lower salt content, 10 mM NaCl versus 134 nm NaCl in PBS. In 10 mM NaCl, the hydrodynamic size of fullerenol was concluded to be 15.7 nm from the intensity distribution. Unfiltered fullerenol samples in 10 mM NaCl exhibited a mean zeta potential distribution of -49.1 ± 2.0 mV (See Supplemental Data). Zeta potential determination provides a measure of the electrostatic potential at the surface of the electrical double layer and the bulk medium, which is related to its surface charge.

Fullerenol Cytotoxicity

LLC-PK1 cell viability 24 and 48 hours post fullerenol exposure was determined with the SRB assay. Fullerenol was cytotoxic to LLC-PK1 cells at concentrations greater than 6 mM at both time points tested (Figure 2). As nanomaterials commonly cause assay interference, the cytotoxic effects of fullerenol were confirmed using the Trypan Blue viability assay. LLC-PK1 cells treated with fullerenol (0.6–60 mM) exhibited a dose-responsive decrease in cell viability 24 hours post fullerenol exposure (See Supplemental Data).

Fullerenol Disrupts the Cytoskeleton and Induces Autophagic Vacuole Accumulation

Actin structure was visualized by confocal microscopy, after staining treated cells with the dye, Oregon Green phalloidin. The actin cytoskeletons of fullerenol treated cells displayed actin filament disruption and clumping, comparable to cells treated with the cytoskeletal protein disruptor, nocodazole (Figure 3).

Fullerenol treated LLC-PK1 cells showed extensive autophagic vacuole accumulation by electron microscopy compared to media control treated cells (Figure 4). For a positive control of autophagy induction, LLC-PK1 cells were treated with starvation medium (Hank's balance salt solution) (Stern *et al.*, 2008). To quantify autophagolysosome accumulation, the fullerenol treated cells and media control treated cells were stained with Lysotracker Red dye, 6, 24, and 48 hours post fullerenol exposure to monitor autolysosome accumulation (Figure 5). Fullerenol treated cells showed dose and time dependent, statistically significant increases in the lysotracker response compared to media control cells, with the most robust Lysotracker Red staining (~250% of control) present 24 hours post 6 mM fullerenol exposure. Fullerenol-autophagy interaction was further confirmed by monitoring LC3-I to LC3-II conversion by western blot, 6 hours and 24 hours post 6 mM fullerenol exposure (Figure 6A–B). The LC3-I to LC3-II conversion was most pronounced following 24 hours of fullerenol exposure (Figure

6B). LC3-I to LC3-II conversion was not monitored at 48 hours due to cytotoxicity at this time point.

Fullerenol Cytotoxicity is Not Associated With Oxidative Stress

For quantitative analysis of fullerenol induced lipid peroxidation, TBARS analysis of lipid peroxidation products released into the media of fullerenol treated versus media control treated cells was conducted 3, 6, and 24 hours post exposure to 3 mM fullerenol (See Supplemental Data). TBARS levels were depressed relative to control at the 3 and 6 hour time points, and were similar to control at the 24 hour time point. Total glutathione levels present in the lysates of fullerenol and media control treated cells were also measured after 3, 6, and 24 hours of exposure to 3 mM fullerenol (See Supplemental Data). A time dependent decrease in glutathione levels was detected in fullerenol treated cells versus media control, with total glutathione levels falling to 80% of control 24 hours after fullerenol treatment. The results of both the TBARS (lack of increase in lipid peroxidation products versus control) and glutathione (minimal decrease in total glutathione) assays suggest minimal oxidative stress following fullerenol treatment, under these assay conditions.

Fullerenol Causes ATP Depletion and Mitochondrial Depolarization

Mitochondria are responsible for efficient coupling of cellular respiration to ATP production. A decline, in ATP levels, therefore is indicative of decreased cellular bioenergetics and is a marker of loss of mitochondrial function. Using a luminescent ATP assay, a dose-dependent decrease in ATP levels were detected in fullerenol (0.2–63.0 mM) treated LLC-PK1 cells in comparison to media control 24 and 48 hr post exposure (Figure 7). This decrease in cellular ATP content occurred at both sub-lethal and lethal fullerenol concentrations.

Two fullerenol concentrations, one which had minimal effects on ATP content (0.3 mM fullerenol) and one that resulted in a dramatic decrease in ATP at both time points (3 mM fullerenol), were chosen as low and high doses, respectively, in confocal analysis of mitochondrial function using Mitotracker Red dye. There was a dramatic loss in Mitotracker Red stain in fullerenol treated cells compared to media control in cells treated with both low and high doses of fullerenol (Figure 8). Uptake of Mitotracker Red dye is dependent upon functional cell mitochondria with intact membrane potentials. The demonstrated loss of Mitotracker Red dye uptake in fullerenol treated cells is indicative of impaired membrane potentials and is consistent with the demonstrated reduction in ATP levels.

3-Methyl Adenine (3-MA) Co-treatment Partially Restores ATP Levels and Mitochondrial Function

3-MA, a class III phostphatidylinositol-3-kinase inhibitor, is a documented suppressor of autophagy (Petiot *et al.*, 2000). Co-treatment of fullerenol with 3-MA, inhibited fullerenol mediated autophagolysosome accumulation and prevented uptake of Lysotracker Red dye (Figure 9). To determine if fullerenol induced ATP depletion and loss of mitochondrial function involved autophagy, ATP levels and Mitotracker Red dye uptake were measured following co-treatment of fullerenol with 3-MA. Co-treatment of cells with 3-MA partially protected against ATP loss resulting from fullerenol treatment alone (Figure 10). Maximal protection resulted in an approximate 20% restoration of ATP loss, a value that was statistically significant. Remarkably, co-treatment of fullerenol with 3-MA also partially restored mitochondrial membrane potential, as measured by Mitotracker Red dye uptake (Figure 8).

Discussion

Fullerenols are attractive molecules for clinical drug delivery, because their hollow caged structure allows for both encapsulation of therapeutic and/or diagnostic loads within the

fullerene cage, and attachment to the scaffolding of the fullerene backbone (Bolskar, 2008). Additionally, derivatization of fullerene to fullerenol enhances its solubility and has been reported to dramatically decrease the toxicity of fullerene in some *in vitro* systems (Sayes, *et al.*, 2004). Thorough evaluation of the biocompatibility and safety of nanotechnology platforms destined for clinical use is imperative (Stern and McNeil, 2008; Hall, *et al.*, 2007). Ideally, characterization of these platforms should include initial screens utilizing *in vitro* systems to identify possible adverse effects and mechanisms of toxicity. Fullerenol toxicity has been demonstrated in numerous animal and human cell lines (Gelderman, *et al.*, 2008, Yamawaki and Iwai, 2006, Sayes *et al.*, 2004, Su *et al.*, 2009). There are, however, no reports in the literature on the cytotoxic effects of fullerenol on kidney cells, and few reports on plausible intracellular targets of this nanomaterial.

Fullerenol nanoparticles used in this present study were purchased commercially. Elemental analysis of fullerenol was conducted by two independent laboratories for molecular formula determination, and fullerenol nanoparticles were tested for metal impurities in our laboratory by ICP-MS (See Supplemental Data). The empirical molecular formula for fullerenol was concluded to be $C_{60}(OH)_{15}(ONa)_9(H_2O)_{15}$ and served as the basis for molecular weight and sample concentration determinations in this study. All fullerenol preparations were virtually free of metal contaminants that could potentially contribute to the biologic and toxic responses observed in this present study (See Supplemental Data). In particular, brominated iron was used as a catalyst during commercial preparation of fullerenol. Quantitative ICP-MS analysis of fullerenol used in this study was determined to contain less than 0.01% of metal iron. Fullerenol preparations were also virtually free of bromine (See Supplemental Data).

Renal cell responses to fullerenol exposure were evaluated in the porcine proximal tubule cell model, LLC-PK1. Carbon based nanomaterials have been documented to interfere with assay markers and cause variable and/or inconclusive assay results in classical toxicology assays (Monteiro-Riviere *et al.*, 2009). Thus, care must be taken to insure that nanoparticles do not cause assay interference. The use of multiple complementary *in vitro* toxicology assays is also advised to confirm nanoparticle effects. In this study, possible fullerenol assay interference was evaluated in all experiments conducted, and when applicable, an orthogonal assay was utilized to confirm study results. Since fullerene derivatives, including fullerenol, can reduce tetrazolium based salts, the traditional MTT and XTT cytotoxicity assays were not used to evaluate cell viability effects in this study.

In this study, treatment of LLC-PK1 cells for 24 and 48 hours with fullerenol in the low millimolar range was cytotoxic, decreasing cell density and compromising the membrane integrity of LLC-PK1 cells, as determined by the SRB assay and Trypan Blue assay, respectively. Interestingly, in a study by Qingnuan, *et al.*, administration of a 1 mg dose of technetium labeled fullerenol ($^{99m}T_c$-$C_{60}(OH)_x$) to mice resulted in retention of approximately 5.25% of the injected dose in the kidney, or a concentration of ~15 mM, at 24 h post fullerenol exposure (Qingnuan *et al.*, 2002). Given these data, the cytotoxic fullerenol concentrations determined here, 6.0 – 60.0 mM, may be relevant to kidney exposures expected *in vivo*.

Fullerenol's mechanism of cell death appears to be cell type specific, and both apoptotic and non-apoptotic mechanisms have been reported in the literature (Yamawaki and Iwai, 2006, Gelderman *et al.*, 2008). Previous studies by other research groups have identified oxidative stress as a primary mechanism of cytotoxicity for underivatized fullerene and nanomaterials in general. Mitochondrial dysfunction induced by fullerenol may be expected to result in ROS production, and oxidative stress. However, fullerenol treatment resulted in only limited oxidative stress in this study, as determined by lipid peroxidation and total glutathione measurement data of fullerenol treated cells. The minimal oxidative stress observed confirms other previous reports that fully hydroxylated fullerenes produce minimal oxygen radicals and

lipid peroxidation products in culture (Sayes *et al.*, 2004, Xia *et al.*, 2006). It is certainly plausible, that in this study, fullerenol attenuated any oxidative stress response resulting from mitochondrial dysfunction by the reported free radical scavenging properties of this nanomaterial.

Fullerenol strongly induced conversion of LC3-I to the autophagy biomarker, LC3-II, in LLC-PK1 cells. LC3-II conversion correlated with lysosomal uptake of Lysotracker Red dye by fullerenol treated cells in both a dose-responsive and time-responsive manner. These results support the use of the Lysotracker Red assay as an initial screen for autophagy interaction following nanoparticle exposure, as reported by our group previously (Stern, *et al.*, 2008.). The robust autophagic response shown here for fullerenol builds upon previous reports of induction of this pathway by fullerene-based nanoparticles (Yamawaki and Iwai, 2006, Zhang *et al.*, 2009, Harhaji *et al.*, 2007). The underlying mechanism(s) responsible for fullerene interaction with the autophagy pathway has not been elucidated. Given that the autophagy response seen here occurred at sub-lethal fullerenol concentrations, it is plausible that autophagy upregulation is a protective cell mechanism intended to remove fullerenol from the cell. With increasing fullerenol concentrations, this autophagic pathway could potentially be overwhelmed as autophagosomes and autophagolysosomes accumulate increasing amounts of fullerenol nanoparticles. To support this hypothesis, future works should include detection of fullerenol within autophagosomes and/or autophagolysosomes for definitive confirmation of uptake of this nanoparticle within autophagy machinery.

There are reports in the literature detailing the effects of carbon-based nanomaterials on actin cytoskeletal structure and organization (Tian, *et al.*, 2006, Walker, *et al.*, 2009). These studies demonstrated compromised actin filament integrity following administration of single- or multi- walled carbon nanotubes in culture. Cytoskeleton disruption may be an initiating event in fullerenol cytotoxicity, as there is evidence that cytoskeleton disruption can interfere with both autophagy processing and mitochondrial capacity.

Cytoskeleton proteins, more specifically, microtubules have been shown to assist in autophagosome formation, movement, and fusion with lysosome (Fass *et al.*, 2006, Kochl *et al.*, 2006). Studies in Saccharomyces cerevisiae (baker's yeast) have identified actin-related protein complexes that target the autophagy transport machinery (Monastyrska, *et al.*, 2008). Recently, a study has suggested a role for actin in mammalian autophagy (Lee *et al.*, 2010). Lee *et al.* have shown that histone deacetylase-6 is involved in autophagosome-lysosome fusion during basal autophagy in mammals, by promoting actin remodeling (Lee *et al.*, 2010).

Nocodazole was used as a positive control in our actin confocal studies. Nocodazole is more commonly used to elicit microtubule disruption, however, there is documented evidence in the literature that this compound also has disruptive effects on the actin cytoskeletal (Takenouchi *et al.*, 2004). Specific interaction and/or binding of fullerenol particles with actin protein was not determined in this study, however given the hydrodynamic size of fullerenol nanoparticles used here, it is expected that this compound can freely diffuse through the cell membrane and enter the cell. It is certainly plausible that fullerenol could bind to actin proteins, thereby potentially affecting actin polymerization and depolymerization states. Interestingly, concentrations of fullerenol that elicited actin filament effects also elicited mitochondrial dysfunction and ATP loss. Induction of mitochondrial dysfunction has also recently been documented for other carbon-based nanoparticles (Yang, *et al.*, 2010).

These data led us to postulate that fullerenol induced cytoskeletal disruption, subsequently disrupts homeostatic mitophagy (mitochondrial specific autophagy) which then leads to mitochondrial dysfunction and ATP depletion, and finally cell death. Elegant studies conducted

in yeast have demonstrated a role for autophagy in mitochondrial maintenance (Zhang, *et al.*, 2007a). These studies showed that yeast strains with mutated autophagy genes had lower oxygen consumption rates, lower mitochondrial membrane potential, high levels of reactive oxygen species (ROS), and an accumulation of dysfunctional mitochondria compared to wild-type yeast strains. The current data suggest that autophagic maintenance of cellular mitochondria may also be important in mammalian cells. The apparent partial recovery of mitochondrial function and ATP levels resulting from 3-MA co-treatment supports this hypothesis. Co-treatment of fullerenol and 3-MA, however, was not sufficient for complete recovery of ATP beyond a maximum restorative value of 20% of control. Autophagy-independent fullerenol-induced cytoskeletal disruption, or direct effects of fullerenol on mitochondrial function, could account for the lack of complete recovery.

There are many other examples from animal and *in vitro* models of human disease that also demonstrate the importance of autophagy in mitochondrial maintenance. For example, the ubiquitin ligase protein, Parkin is often mutated in familial forms of Parkinson disease and appears to play a role in recruitment of damaged mitochondria for autophagic degradation (Narendra *et al.*, 2009). Knockout of Parkin in mice results in loss of mitochondrial function (Palacino *et al.*, 2004). Excessive autophagy, resulting from either unregulated induction or blocked autophagosome cycling, can also have a detrimental effect on mitochondria. In a mouse model of the lysosomal storage disorder G(M1)-gangliosidosis, knockout of the lysosomal beta-galactosidase enzyme in mice resulted in autophagosome accumulation and loss of mitochondrial membrane potential, that were ameliorated by treatment with the autophagy inhibitor, 3-methyladenine (Takamura *et al.*, 2008). In an *in vitro* model of neurodegeneration, nerve growth factor withdrawal from primary neurons in culture resulted in cytoskeleton disruption, autophagosome accumulation and loss of mitochondrial membrane potential (Yang *et al.*, 2007). The disruption of mitochondrial membrane potential by nerve growth factor withdrawal could be prevented by treatment with the autophagy inhibitor 3-methyladenine.

In addition to autophagy-mediated mitochondrial dysfunction, there is also ample evidence that actin cytoskeleton disruption itself can interfere with mitochondrial capacity directly (Anesti and Scorrano, 2006). For example, yeast mutants with actin instability, displaying a clumped actin phenotype similar to that observed following treatment of LLC-PK1 cells with fullerenol, also had greatly reduced mitochondrial membrane potential (Gourlay *et al.*, 2004). A study in neuroblastoma cells demonstrated that disorganization of the actin cytoskeleton by overexpression of transgelin coincided with mitochondria depolarization (Ward *et al.*, 2010).

Lastly, it is important to note that a direct fullerenol mitochondrial mechanism may be involved in this study, with fullerenol-induced mitochondrial damage resulting in mitophagy induction, disruption of actin cytoskeleton, and apoptotic cell death. Indeed, there is evidence of direct inhibition of mitochondrial function by fullerenol (Ueng *et al.*, 1997). Mitochondria have been reported to serve as a switch between apoptosis and autophagy, with increasing levels of stress resulting in the initial induction of mitophagy, followed by caspase activation, apoptotic cell death, and finally necrotic cell death under the most extreme stress conditions (Nishida *et al.*, 2008). Initial induction of mitophagy by the cell to clear damaged mitochondria is consistent with the fact that in this study, there is evidence of autophagy induction at sub-lethal fullerenol concentrations (Figures 4 and 5) that are approximately one order of magnitude lower than fullerenol concentrations that induced ATP depletion (Figure 7) and mitochondrial dysfunction (Figure 8). Furthermore, the TEM image of fullerenol treated cells shows the presence of damaged mitochondria (Figure 4). With increasing fullerenol concentrations, possible direct fullerenol effects on cytoskeletal structure could serve as a negative feedback mechanism to stall stress-induced mitophagy (cause mitophagy dysfunction) and trigger cell death. Alternatively, direct fullerenol-induced mitochondrial damage could result in downstream

disruption of actin cytoskeleton structure due to alteration in calcium homeostasis (Nicotera *et al.*, 1992) and/or diminished cellular bioenergetics (Molitoris *et al.*, 1996).

In summary, fullerenol cytotoxicity in the LLC-PK1 cells was associated with cytoskeleton disruption, autophagic vacuole accumulation, and mitochondrial dysfunction. Fullerenol-induced ATP depletion and loss of mitochondrial potential were partially ameliorated by cotreatment with the autophagy inhibitor, 3-methyladenine. As there is evidence that cytoskeleton disruption can interfere with both autophagy processing and mitochondrial capacity, it is hypothesized that cytoskeleton disruption may be an initiating event in fullerenol cytotoxicity, leading to subsequent autophagy dysfunction, and loss of mitochondrial capacity. While this proposed mechanism is consistent with the data presented, other mechanisms are certainly plausible, as discussed above. Nanoparticle-induced cytoskeleton disruption, as well as autophagy and mitochondrial dysfunctions, have been reported commonly in the literature, suggesting the proposed mechanism of fullerenol toxicity may be relevant for a variety of nanomaterials. It is important to note, however, that nanomaterials as a class include highly varied physicochemical characteristics, thus it would not be appropriate to attribute this mechanism of fullerenol toxicity to the entire class.

Supplementary Material

Refer to Web version on PubMed Central for supplementary material.

Acknowledgments

The authors would like to thank Jamie Rodriguez for assistance with the LC3 immunoblot and Timothy Potter for assistance with cell culture. This project has been funded in whole or in part with federal funds from the National Cancer Institute, National Institutes of Health, under contract HHSN261200800001E. The content of this publication does not necessarily reflect the views or policies of the Department of Health and Human Services, nor does mention of trade names, commercial products, or organizations imply endorsement by the U.S. Government.

References

Anderson SA, Lee KK, Frank JA. Gadolinium-fullerenol as a paramagnetic contrast agent for cellular imaging. Invest. Radiol 2006;41:332–338. [PubMed: 16481917]

Anesti V, Scorrano L. The relationship between mitochondrial shape and function and the cytoskeleton. Biochim. Biophys. Acta 2006;1757:692–699. [PubMed: 16729962]

Bensasson RV, Brettreich M, Frederiksen J, Göttinger H, Hirsch A, Land EJ, Leach S, McGarvey DJ, Schönberger H. Reactions of e–aq, CO2●–, HO●, O2● – and O2(1g) with a Dendro[60] Fullerene and C60 [C(COOH)2]n (n_ 2_6). Free Radical. Biol. Med 2000;29:26–33.

Bolskar RD. Gadofullerene MRI contrast agents. Nanomedicine 2008;3:201–213. [PubMed: 18373426]

Chaudhuri P, Paraskar A, Soni S, Mashelkar RA, Sengupta S. Fullerenol-cytotoxic conjugates for cancer chemotherapy. ACS Nano 2009;3:2505–2514. [PubMed: 19681636]

Dugan LL, Turetsky DM, Du C, Lobner D, Wheeler M, Almli CR, Shen CK-F, Luh T-Y, Choi DW, Lin T-S. Carboxyfullerenes as Neuroprotective Agents. Proc. Natl. Acad. Sci. U.S.A 1997;94:9434–9439. [PubMed: 9256500]

Fass E, Shvets E, Degani I, Hirschberg K, Elazar Z. Microtubules support production of starvation-induced autophagosomes but not their targeting and fusion with lysosomes. J. Biol. Chem 2006;281:36303–36316. [PubMed: 16963441]

Gharbi N, Pressac M, Hadchouel M, Szwarc H, Wilson SR, Moussa F. [60] Fullerene is a powerful antioxidant in vivo with no acute or subacute toxicity. Nano Lett 2005;5:2578–2585. [PubMed: 16351219]

Gelderman MP, Simakova O, Clogston JD, Patri AK, Siddiqui SF, Vostal AC, Simak J. Adverse effects of fullerenes on endothelial cells: Fullerenol $C_{60}(OH)_{24}$ induced tissue factor and ICAM-1 membrane expression and apoptosis in vitro. Int. J. Nanomed 2008;3:59–68.

Gourlay CW, Carpp LN, Timpson P, Winder SJ, Ayscough KR. A role for the actin cytoskeleton in cell death and aging in yeast. J. Cell. Biol 2004;164:803–809. [PubMed: 15024029]

Hall JB, Dobrovolskaia MA, Patri AK, McNeil SE. Characterization of nanoparticles for therapeutics. Nanomedicine 2007;2:789–803. [PubMed: 18095846]

Harhaji L, Isakovic A, Raicevic N, Markovic Z, Todorovic-Markovic B, Nikolic N, Vranjes-Djuric S, Markovic I, Trajkovic V. Multiple mechanisms underlying the anticancer action of nanocrystalline fullerene. Eur. J. Pharmacol 2007;568:89–98. [PubMed: 17560995]

Injac R, Perse M, Boskovic M, Djordjevic-Millic V, Djordjevic A, Hvala A, Cerar A, Strukelj B. Cardioprotective effects of fullerenol C60(OH)24 on a single dose doxorubicin-induced cardiotoxicity in rats with malignant neoplasm. Technol. Can. Res. Treat 2008a;7:15–25.

Injac R, Perse M, Obermajer N, Djordjevic-Milic V, Prijatelj M, Djordjevic A, Cerar A, Strukelj B. Potential hepatoprotective effects of fullerenol C60(OH)24 in doxorubicin-induced hepatotoxicity in rats with mammary carcinomas. Biomaterials 2008b;29:3451–3460. [PubMed: 18501960]

Injac R, Boskovic M, Perse M, Koprivec-Furlan E, Cerar A, Djordjevic A, Strukelj B. Acute doxorubicin nephrotoxicity in rats with malignant neoplasm can be successfully treated with fullerenol $C_{60}(OH)_{24}$ via suppression of oxidative stress. Pharm. Rep 2008c;60:742–749.

Injac R, Perse M, Cerne M, Potocnik N, Radic N, Govedarica B, Djordjevic A, Cerar A, Strukelj B. Protective effects of fullerenol $C_{60}(OH)_{24}$ against doxorubicin-induced cardiotoxicity and hepatotoxicity in rats with colorectal cancer. Biomaterials 2009;30:1184–1196. [PubMed: 19046599]

Klionsky DJ, Cuervo AM, Seglen PO. Methods for monitoring autophagy from yeast to human. Autophagy 2007;3:181–206. [PubMed: 17224625]

Kochl R, Hu XW, Chan EYW, Tooze SA. Microtubules facilitate autophagosome formation and fusion of autophagosomes with endosomes. Traffic 2006;7:129–145. [PubMed: 16420522]

Lee J, Koga H, Kawaguchi Y, Tang W, Wong E, Gao YS, Pandey UB, Kaushik S, Tresse E, Lu J, Taylor JP, Cuervo AM, Yao TP. HDAC6 controls autophagosome maturation essential for ubiquitin-selective quality-control autophagy. EMBO 2010;29:969–980.

Molitoris BA, Dahl R, Hosford M. Cellular ATP depletion induces disruption of the spectrin cytoskeletal network. Am. J. Physiol 1996;271:F790–F798. [PubMed: 8898008]

Monastyrska I, He C, Geng J, Hoppe AD, Li Z, Klionsky DJ. Arp2 links autophagic machinery with the actin cytoskeleton. Mol. Biol. Cell 2008;19:1962–1975. [PubMed: 18287533]

Monteiro-Riviere NA, Inman AO, Zhang LW. Limitations and relative utility of screening assays to assess engineered nanoparticle toxicity in a human cell line. Toxicol. Appl. Pharmacol 2009;234:222–235. [PubMed: 18983864]

Narendra D, Tanaka A, Suen DF, Youle RJ. Parkin-induced mitophagy in the pathogenesis of Parkinson disease. Autophagy 2009;5:706–708. [PubMed: 19377297]

Nicotera P, Bellomo G, Orrenius S. Calcium-mediated mechanisms in chemically induced cell death. Annu. Rev. Pharmacol. Toxicol 1992;32:449–470. [PubMed: 1605574]

Nishida K, Yamaguchi O, Otsu K. Crosstalk between autophagy and apoptosis in heart disease. Circulation Research 2008;103:343–351. [PubMed: 18703786]

Okuda K, Mashino T, Hirobe M. Superoxide Radical Quenching and Cytochrome C Peroxidase-like Activity of C60-Dimalonic Acid, C62(COOH)4. Bioorg. Med. Chem. Lett 1996;6:539–542.

Peer D, Karp JM, Hong S, Farokhzad OC, Margalit R, Langer R. Nanocarriers as an emerging platform for cancer therapy. Nature Nanotechnology 2007;2:751–760.

Petiot A, Ogier-Denis E, Blommaart EF, Meijer AJ, Codogno P. Distinct classes of phosphatidylinositol 3'-kinases are involved in signaling pathways that control macroautophagy in HT-29 cells. J. Biol. Chem 2000;275:992–998. [PubMed: 10625637]

Pfaller W, Gstraunthaler G. Nephrotoxicity testing in vitro- what we know and what we need to know. Env. Health Perspect 1998;106:559–569. [PubMed: 9599703]

Perazella MA. Renal vulnerability to drug toxicity. Clin. J. Amer. Soc. Nephro 2009;4:1275–1283.

Palacino JJ, Sagi D, Goldberg MS, Krauss S, Motz C, Wacker M, Klose J, Shen J. Mitochondrial dysfunction and oxidative damage in parkin-deficient mice. J. Biol. Chem 2004;279:18614–18622. [PubMed: 14985362]

Qingnuan L, Yan X, Xiaodong Z, Ruili L, Qieqie D, Xiaoguang S, Shaoliang C, Wenxin L. Preparation of ^{99}Tm-$C_{60}(OH)_x$ and its biodistribution studies. Nuc. Med. Radiol 2002;29:707–710.

Rodriguez-Enriquez S, Kim I, Currin RT, Lemasters JJ. Tracker dyes to probe mitochondrial autophagy (mitophagy) in rat hepatocytes. Autophagy 2006;2:39–46. [PubMed: 16874071]

Sayes CM, Fortner JD, Guo W, Lyon D, Boyd AM, Ausman KD, Tao YJ, Sitharaman B, Wilson LJ, Hughes JB, West JL, Colvin VL. The differential cytotoxicity of water soluble fullerenes. Nano Lett 2004;4:1181–1887.

Shaik IH, Mehvar R. Rapid determination of reduced and oxidized glutathione levels using a new thiol-masking reagent and the enzymatic recycling method: application to the rat liver and bile samples. Anal. Bional. Chem 2006;385:105–113.

Stern ST, McNeil SE. Nanotechnology safety concerns revisited. Toxicol. Sci 2008;101:4–21. [PubMed: 17602205]

Stern ST, Zolnik BS, McLeland CB, Clogston J, Zheng J, McNeil SE. Induction of autophagy in porcine kidney cells by quantum dots: A common cellular response to nanomaterials? Toxicol. Sci 2008;106:140–152. [PubMed: 18632727]

Su Y, Xu J, Shen P, Li J, Wang L, Li Q, Li W, Xu G, Fan C, Huang Q. Cellular uptake and cytotoxic evaluation of fullerenol in different cell lines. Toxicology 2010;269:155–159. [PubMed: 19941929]

Takamura A, Higaki K, Kajimaki K, Otuska S, Ninomiya H, Matsuda J, Ohno K, Suzuki Y, Nanba E. Enhanced autophagy and mitochondrial aberrations in murine G(M1)-ganliosidosis. Biochem. Biophys. Res. Commun 2008;367:616–622. [PubMed: 18190792]

Takenouchi T, Miyashita N, Ozutsumi K, Rose MT, Aos H. Role of caveolin-1 and cytoskeletal proteins, actin, and vimentin, in adipogenesis of bovine intramuscular preadipocyte cells. Cell Biol. Int 2004;28:615–623. [PubMed: 15350596]

Tian F, Cui D, Schwarz H, Estrada GG, Kobayashi H. Cytotoxicity of single-wall carbon nanotubes on human fibroblasts. Toxicol. In Vitro 2006;20:1202–1212. [PubMed: 16697548]

Ueng TH, Kang JJ, Wang HW, Cheng YW, Chiang L-Y. Suppression of microsomal cytochrome P450-dependent monooxygenases and mitochondrial oxidative phosphorylation by fullerenol, a polyhydroxylated fullerene C60. Toxicol. Lett 1997;93:29–37. [PubMed: 9381480]

Verbeeck RK, Musuamba FT. Pharmacokinetics and dosage adjustment in patients with renal dysfunction. Eur. J. Clin. Pharmacol 2009;65:757–773. [PubMed: 19543887]

Walker VG, Li Z, Hulderman T, Schwegler-Berry D, Kashon ML, Simeonova PP. Potential in vitro effects of carbon nanotubes on human aortic endothelial cells. Toxicol. Appl. Pharmacol 2009;236:319–328. [PubMed: 19268679]

Wang IC, Tai LA, Lee DD, Kanakamma PP, Shen CK-F, Luh T-Y, Cheng CH, Hwang KC. C60 and Water-Soluble Fullerene Derivatives as Antioxidants Against Radical-Initiated Lipid Peroxidation. J. Med. Chem 1999;42:4614–4620. [PubMed: 10579823]

Ward MW, Concannon CG, Whyte J, Walsh CM, Corley B, Prehn JH. The amyloid precursor protein intracellular domain (AICD) disrupts actin dynamics and mitochondrial bioenergetics. J. Neurochem 2010;113:275–284. [PubMed: 20405578]

Williams PD. The application of renal cells in culture in studying drug-induced nephrotoxicity. In Vitro Cell Dev. Biol 1989;25:800–805. [PubMed: 2793779]

Wey HE, Pyron L, Woolery M. Essential fatty acid deficiency in cultured human keratinocytes attenuates toxicity due to lipid peroxidation. Toxicol. Appl. Pharmacol 1993;120:72–79. [PubMed: 8511784]

Xiao L, Takada H, Maeda K, Haramoto M, Miwa N. Antioxidant Effects of Water-Soluble Fullerene Derivatives against Ultraviolet Ray or Peroxylipid through Their Action of Scavenging the Reactive Oxygen Species in Human Skin Keratinocytes. Biomed. Pharmacother 2005;59:351–358. [PubMed: 16087310]

Xia T, Kovochich M, Brant J, Hotze M, Sempf J, Oberley T, Sioutas C, Yeh JI, Weisner MR, Nel AE. Comparison of the abilities of ambient and manufactured nanoparticles to induce cellular toxicity according to an oxidative stress paradigm. Nano Lett 2006;6:1794–1807. [PubMed: 16895376]

Xing G, Zhang J, Zhao Y, Tang J, Zhang B, Gao X, Yuan H, Qu Li, Cao W, Chai Z, Ibrahim K, Su R. Influences of structural properties on stability of fullerenols. J. Phys. Chem. B 2004;108:11473–11479.

Yamago S, Tokuyama H, Nakamura E, Kikuchi K, Kananishi S, Sueki K, Nakahara H, Enomoto S, Ambe F. In vivo biological behavior of a water-miscible fullerene: 14C labeling, absorption, distribution, excretion and acute toxicity. Chem. and Biol 1995;2:385–389. [PubMed: 9383440]

Yamawaki H, Iwai N. Cytotoxicity of water-soluble fullerene in vascular endothelial cells. Am. J. Physiol. Cell Physiol 2006;290:1495–1502.

Yang Y, Fukui. K, Koike T, Zheng X. Induction of autophagy in neurite degeneration of mouse superior cervical ganglion neurons. Eur. J. Neurosci 2007;26:2979–2988. [PubMed: 18001292]

Yang Z, Zhang Y, Yang Y, Sun L, Han D, Li H, Wang C. Pharmacological and toxicological target organelles and safe use of single-walled carbon nanotubes as drug carriers in treating Alzheimer disease. Nanomed. Nanotechnol. 2010 doi:10.1016/j.nano.2009.11.007.

Zhang Y, Qi H, Taylor R, Xu W, Liu LF, Jin S. The role of autophagy in mitochondria maintenance. Autophagy 2007a;3:337–346. [PubMed: 17404498]

Zhang J, Liu K, Xing G, Ren T, Wang S. Synthesis and in vivo study of metallofullerene based MRI contrast agent. J. Radioanal. Nuc. Chem 2007b;272:605–609.

Zhang Q, Yang W, Man N, Zheng F, Shen Y, Sun K, Yang L, Wen L-P. Autophagy-mediated chemosensitization in cancer cells by fullerene C60 nanocrystal. Autophagy 2009;5:1–11.

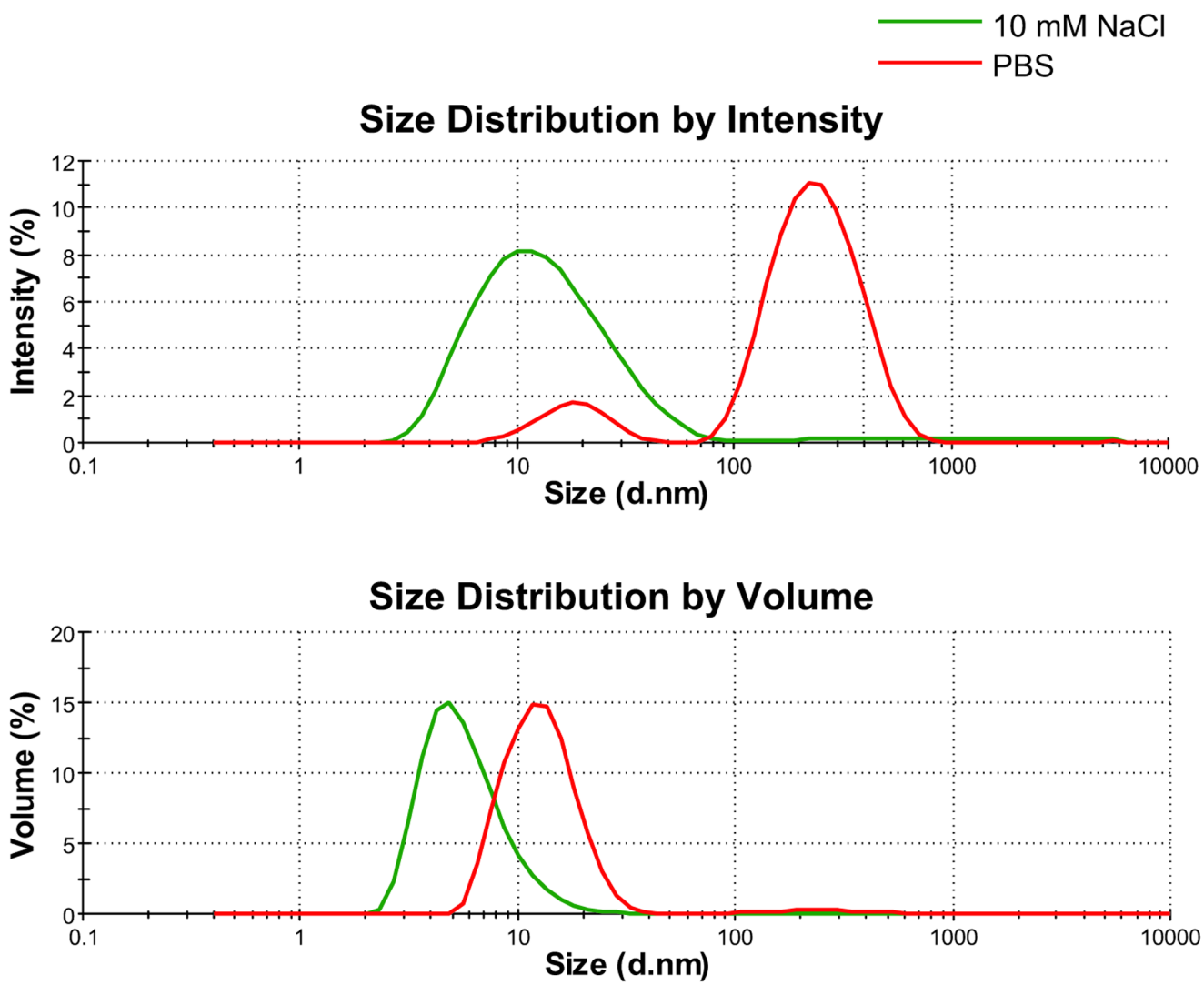

Figure 1. Hydrodynamic Size Analysis by DLS

Shown are the intensity and volume distributions of fullerenol-PBS (**red**) and fullerenol-10 mM NaCl (**green**) preparations. Each distribution line is the average of 12 independent measurements. Intensity-weighted average was used to determine hydrodynamic size, while volume distribution data was used to determine relative amounts.

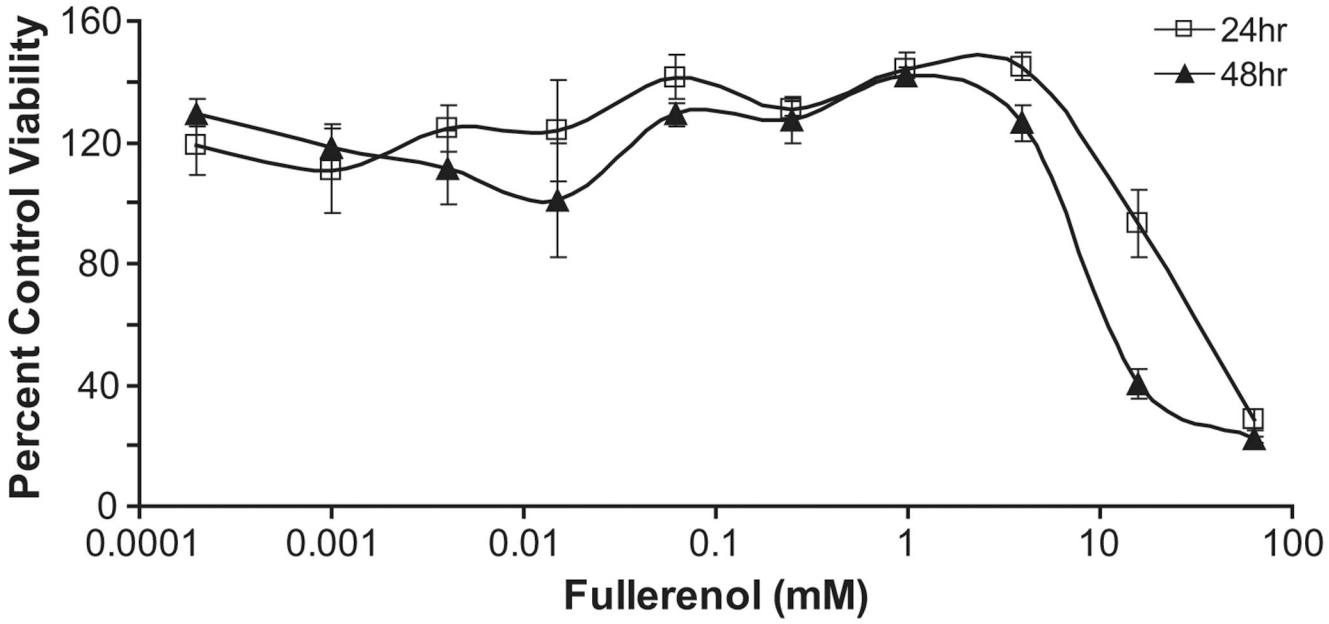

Figure 2. SRB Viability

LLC-PK1 cells were treated for 24 and 48 hrs with 0.0002– 60 mM fullerenol. Cell viability was determined at each time point by the SRB assay. Data are presented as percent media control cell viability. Values correspond to the mean ± SE, N=3.

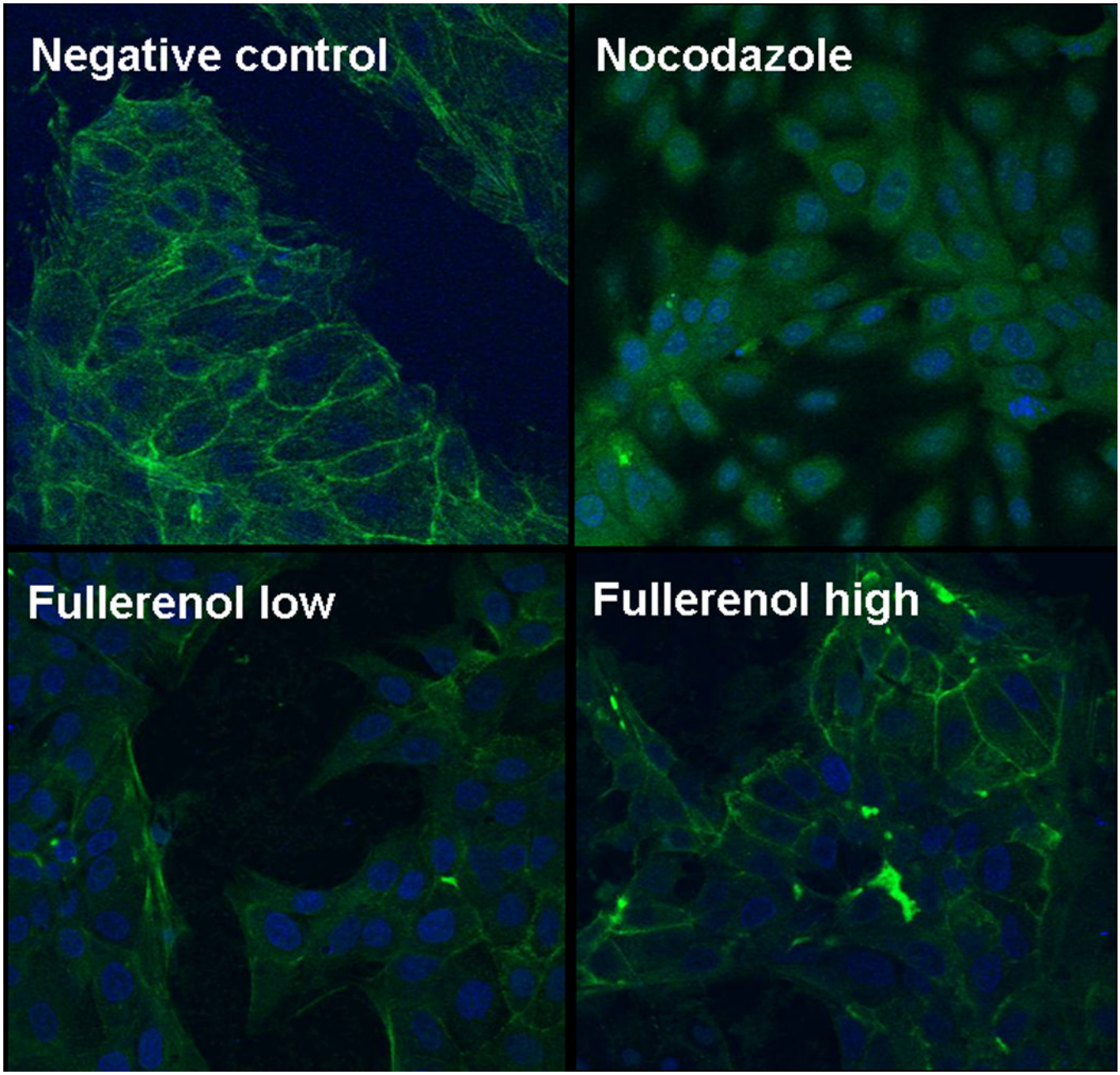

Figure 3. Fullerenol Actin Confocal Analysis

LLC-PK1 cells grown on cover slips were treated for 24 hrs with media (negative control), low dose fullerenol (0.6 mM), high dose fullerenol (3 mM), or were pre-treated with nocodazole (50.0 μM) for 2 hrs. All cells were stained with 1 unit (fluorescence) of Oregon Green 488 phalloidin dye/Hoechst nuclear stain/coverslip (20 μL of 6.6 uM methanolic Oregon Green stock solution/5 μg Hoechst/mL of 1% BSA-PBS /coverslip) for 20 min at ambient temperature, and were attached to microscope slides prior to confocal analysis. Images were acquired at 40× (oil) magnification.

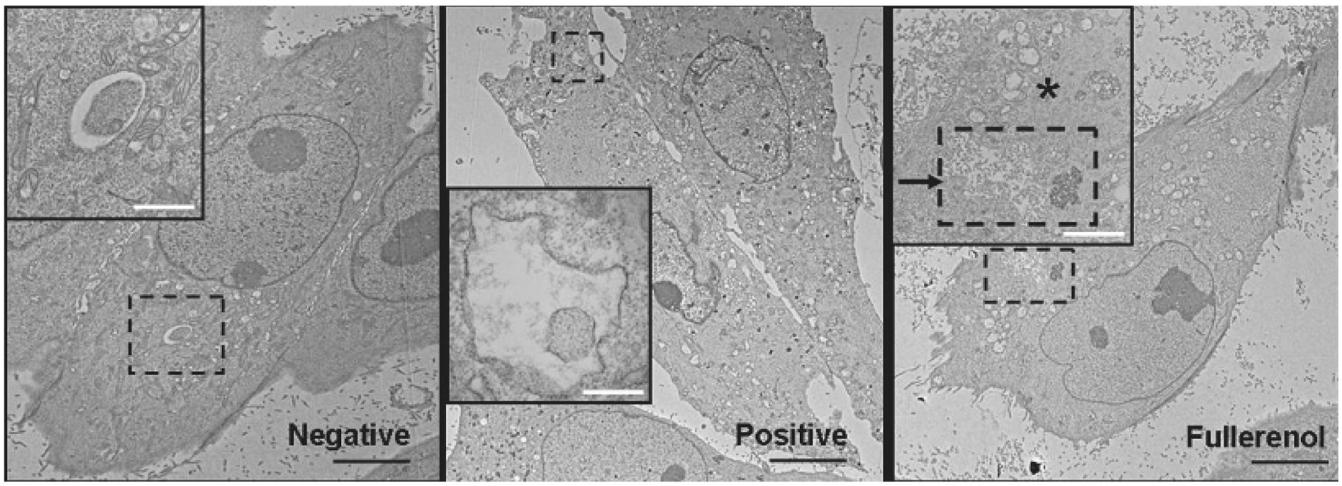

Figure 4. TEM Photomicrographs

LLC-PK1 cells were treated for 6 hrs with media (negative), Hank's balanced salt starvation media (positive), or 0.03 mM fullerenol (treated). Black inlet boxes show autophagic vacuoles, consisting of double layered membranes containing cellular debris. Image scale bar lengths are as follows: Black scale bar is 10 μm, negative inset bar is 1 μm, positive inset bar is 10 nm and fullerenol inset bar is 2 μm. Asterisk indicates mitochondrial damage. Images were acquired at 5,000–20,000× magnification.

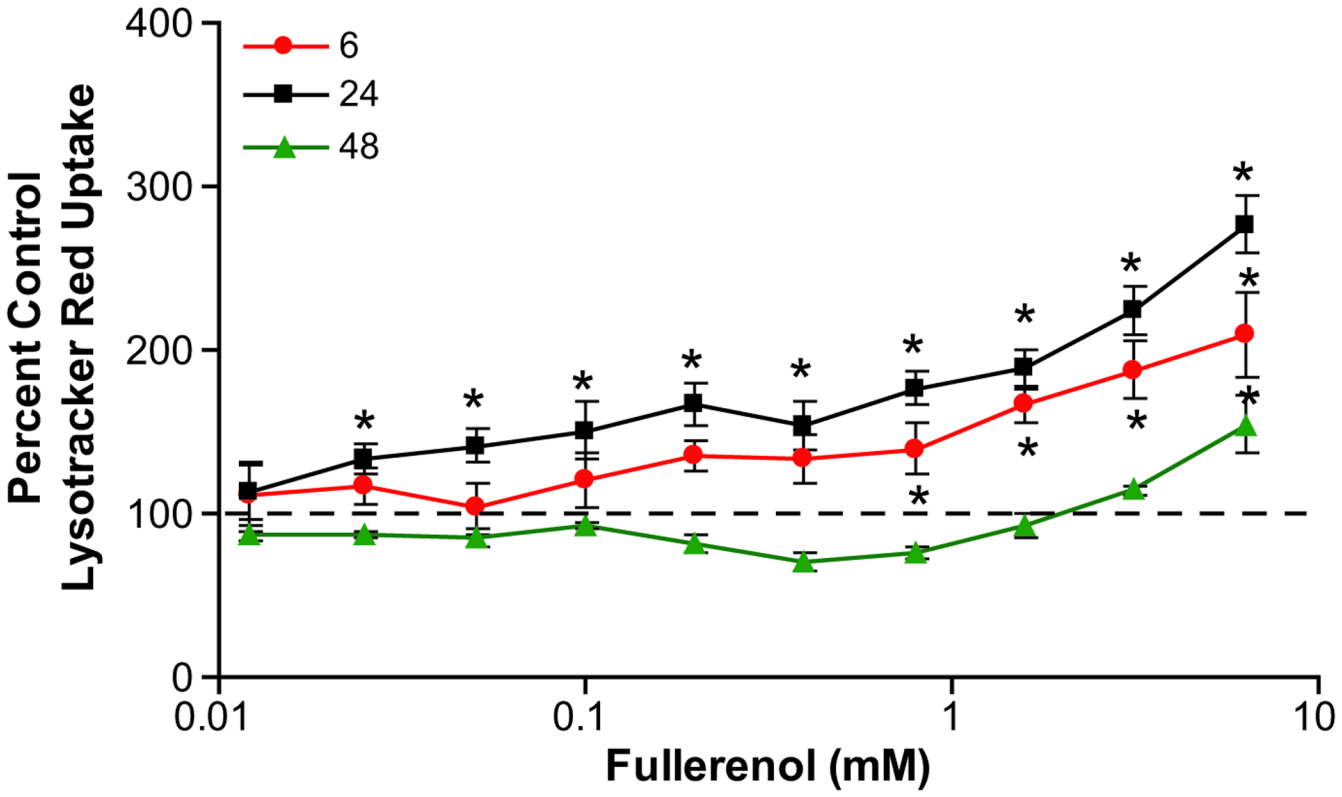

Figure 5. Lysotracker Response

LLC-PK1 cells were treated for 6, 24 or 48 hrs with 0.01–6 mM fullerenol. Data are presented as the percent control Lysotracker Red fluorescence normalized to Celltracker Green fluorescence (percent control Lysotracker red fluorescence/percent control Celltracker green fluorescence). Values correspond to mean ± SE of 3 individual samples. Asterisks indicate statistical difference from control (ANOVA, Dunnett's post hoc, $p < 0.05$).

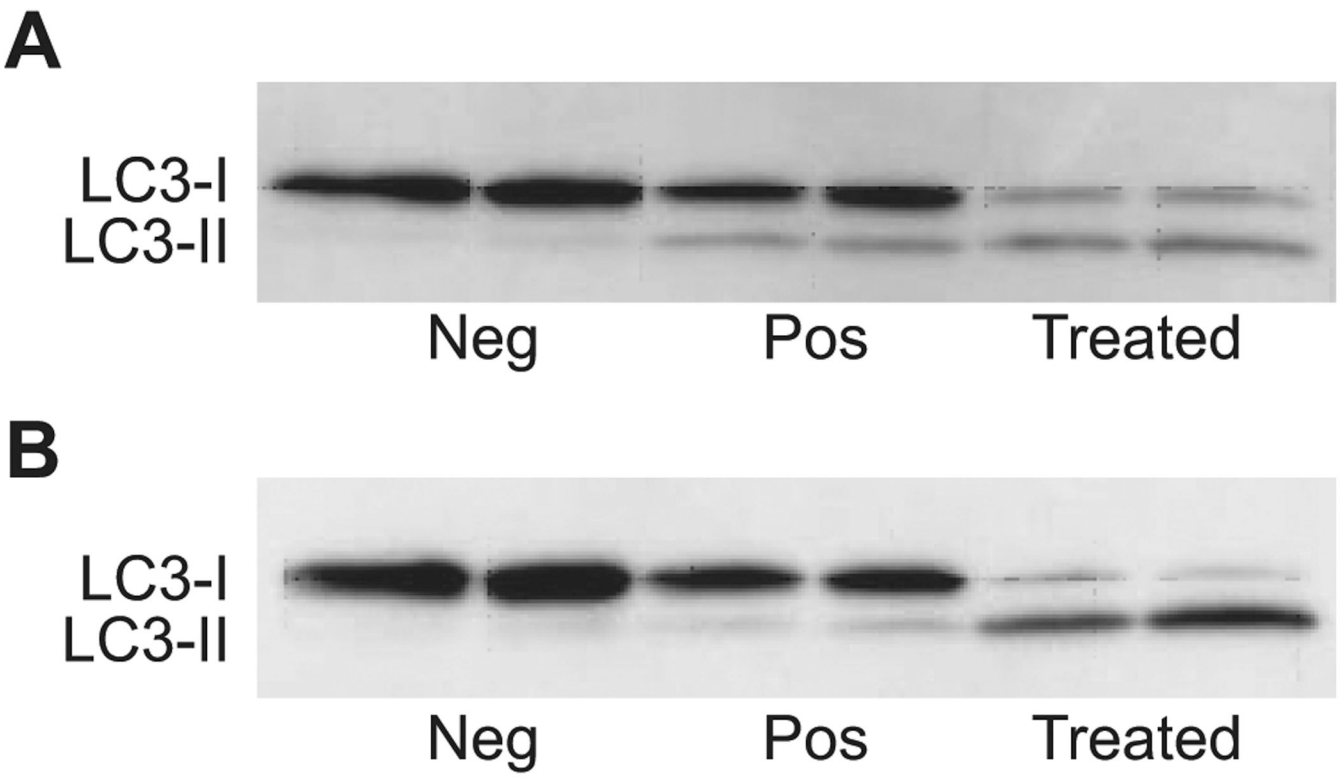

Figure 6. LC3 Immunoblot

LLC-PK1 cells were treated for 6 hrs (A) and 24 hrs (B) with media (negative), starvation buffer (positive), or 6 mM fullerenol (treated) in duplicate. Cell lysate proteins were separated by SDS-PAGE, transferred to PVDF membrane, and probed for LC3 reactive proteins. LC3-I and II are labeled on the immunoblots.

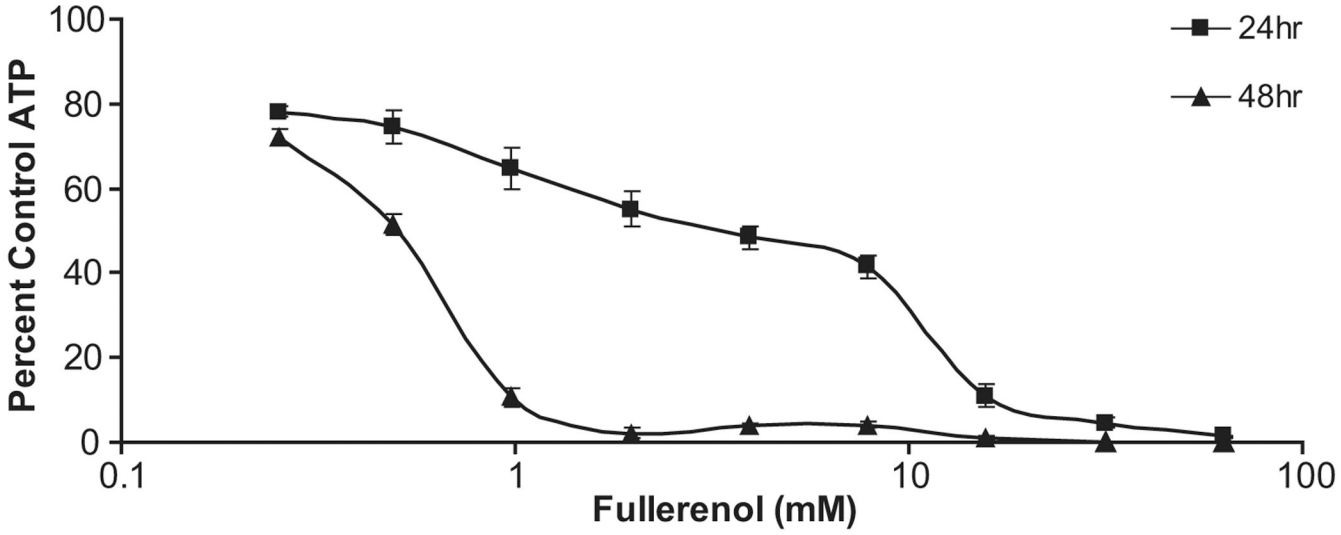

Figure 7. Fullerenol ATP Assay

LLC-PK1 cells were treated for 24 and 48 hrs with 0.2–60 mM fullerenol. ATP content was determined at each time point by the luciferin-luciferase assay. Data are presented as percent media control. Values correspond to the mean ± SE, N=3.

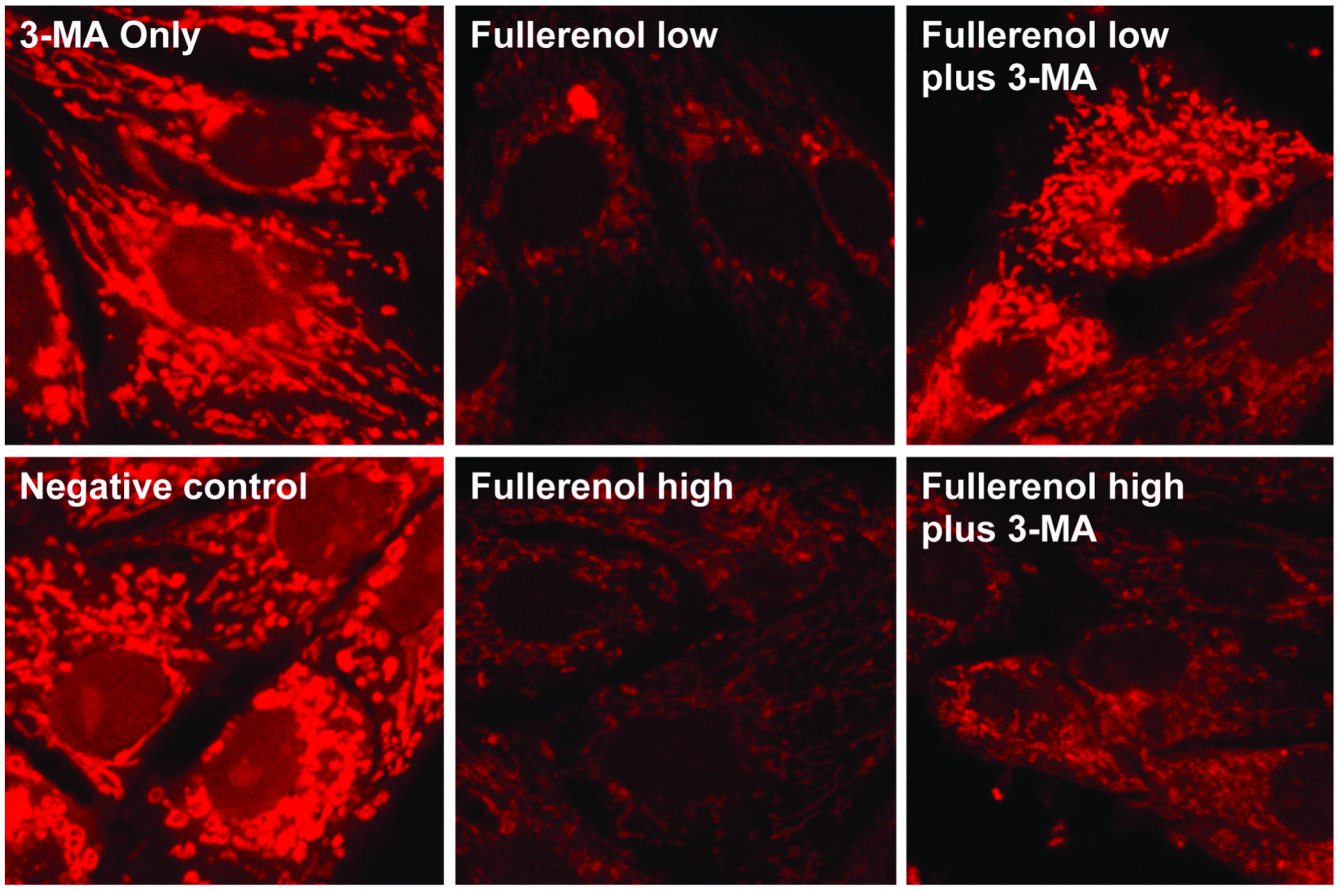

Figure 8. Fullerenol plus 3-MA Mitochondrial Confocal Analysis

LLC-PK1 cells grown on cover slips were treated for 24 hrs with media (negative control), low dose fullerenol (0.6 mM), or high dose fullerenol (3 mM), with or without pretreatment with 2 mM 3-methyladenine (3-MA) for 2 hrs, prior to 1 mM 3-MA cotreatment. All cells were stained with 200 nM Mitotracker Red, fixed with 4 % formaldehyde, and were attached to microscope slides prior to confocal analysis. Images were acquired at 148× (oil) magnification under identical detector settings.

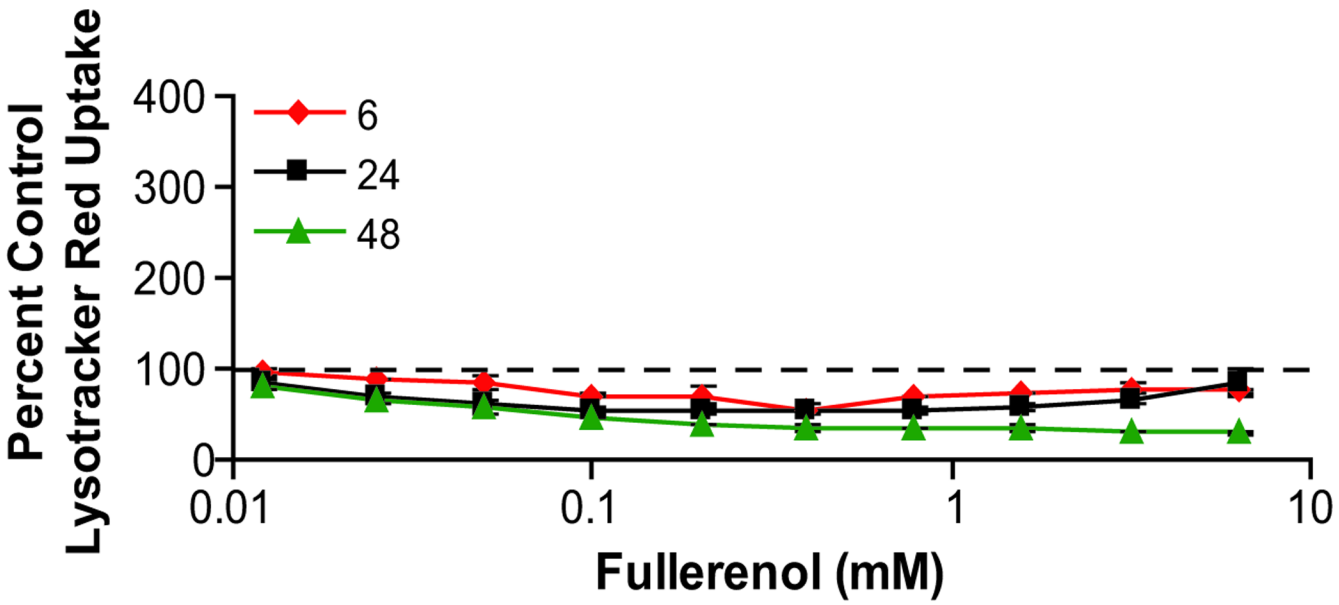

Figure 9. Fullerenol plus 3-MA Lysotracker Assay

LLC-PK1 cells were pre-treated with 2 mM 3-methyladenine (3-MA) for 2 hrs, prior to 0.01–6 mM fullerenol and 1 mM 3-MA cotreatment for an additional 6, 24 and 48 hrs. Data are presented as the percent control Lysotracker Red fluorescence normalized to Celltracker Green fluorescence (percent control Lysotracker red fluorescence/percent control Celltracker green fluorescence). Values correspond to mean ± SE of 3 individual samples.

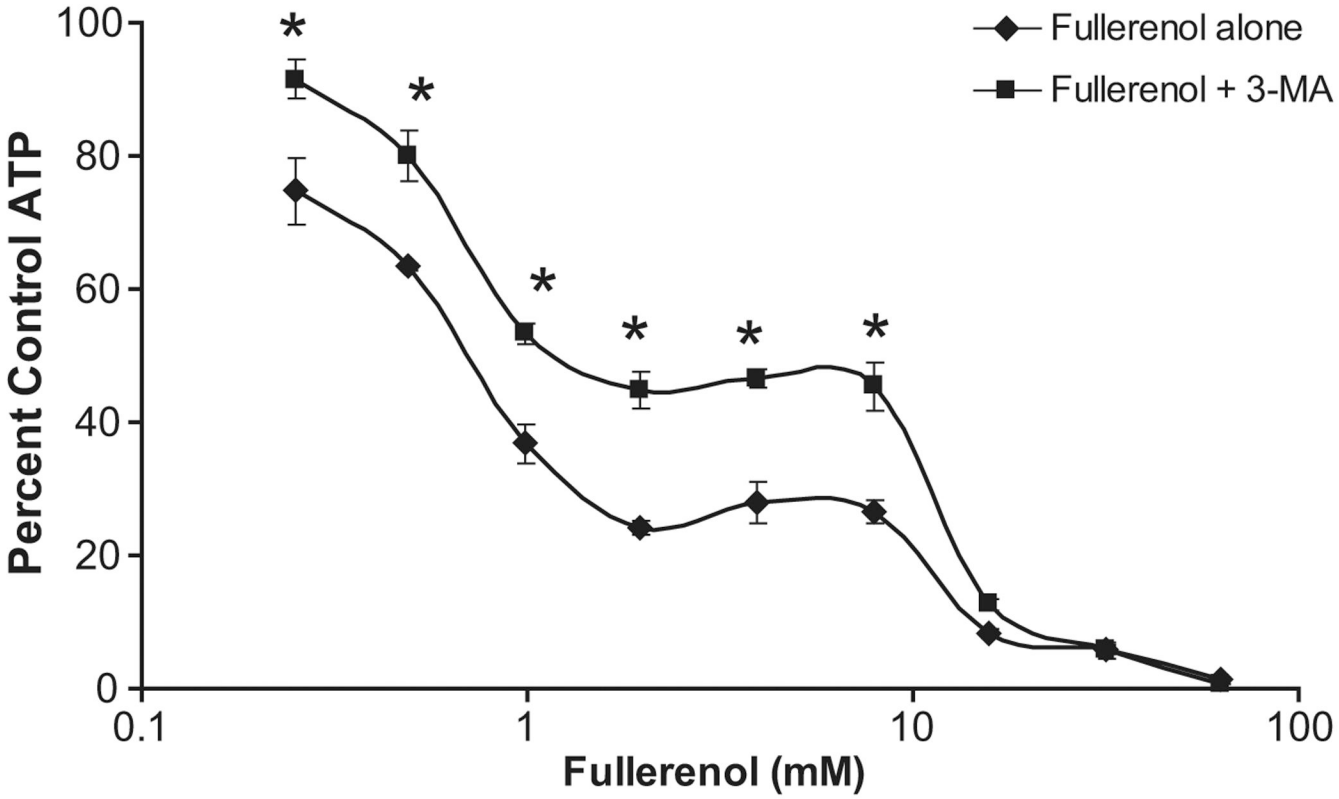

Figure 10. Fullerenol plus 3-MA ATP Assay

LLC-PK1 cells were treated for 24 and 48 hrs with 0.2–60 mM fullerenol, with or without pre-treatment with 2 mM 3-methyladenine (3-MA) for 2 hrs prior to 1 mM 3-MA cotreatment. ATP content was determined at each time point by the luciferin-luciferase assay. Data are presented as percent media control ATP level. Values correspond to the mean ± SE, N = 3. Asterisks indicate statistical difference from fullerenol alone treatment (Student's t-test, $p < 0.05$).